Energy-Efficient Design of Broad Beams for Massive MIMO Systems

Sven O. Petersson, and Maksym A. Girnyk

***Abstract*—Massive MIMO is a promising air interface technology for 5G wireless communications. Such antenna systems offer capabilities to utilize channel correlations to create beams suitable for user specific transmissions. Most of the prior research is devoted to user-specific transmission in such systems, where a narrow beam is formed towards a user to improve its reception. Meanwhile, public-channel transmission to multiple users at once by means of broad beams has been understudied. In this paper, we introduce the concept of *array-size invariant* (ASI) beamforming, enabling generation of broad beams from very large antenna arrays where all elements are transmitting at maximum power. The ASI technique offers the possibility to achieve a perfectly flat array factor by exploiting the additional degree of freedom coming from the dual-polarization beamforming. The proposed technique is applicable to both uniform linear and rectangular arrays. The benefits of the method are shown by means of several numerical examples. In particular, the practical usefulness of the ASI beamforming, in terms of coverage and energy efficiency, is illustrated on a example of designing a cell-specific broad beam for public-channel transmission in a realistic network deployment.**

***Index Terms*—Array-size invariant beamforming, dual-polarization beamforming, beam design, broad beam.**

I. Introduction

ONE of the main goals of mobile communication systems have, for many years, been to increase user data rates and system throughput. One of the means for making this happen has been the increase of the number of antennas in order to more efficiently utilize the spatial domain. Various transmission schemes for dedicated channels for exchange of user-specific data have been investigated and standardized in 5G New Radio (NR), see [1] for an overview.

Meanwhile, another important aspect of multi-antenna technology that has received less attention is transmission in the absence of channel state information (CSI), often referred to as *broad-beam* transmission. Such transmission is suitable for public channels, such as, e.g., Physical Downlink Control Channel (PDCCH) and Physical Broadcast Channel (PBCH), for broadcasting cell-specific reference and synchronization signals. Typical requirements on such transmission are a broad radiation pattern and equal power per antenna. Unfortunately, designing beams with such characteristics is not straightforward. It is well known that feeding all elements in an antenna array with the same amplitude and phase results in a narrow beam, potentially much narrower than the angular region in which the served users are located. For instance, 4G Long-Term Evolution (LTE) specifies *discrete Fourier transform* (DFT) based codebooks [2] for user-specific beamforming. To broadcast common signals a codebook's beams may be swept over, which is referred to as the grid-of-beams method [3]. The size of the grid can furthermore be reduced by exploiting orthogonal basis functions [4] or reformulating the search as a non-monotone submodular maximization problem [5]. Such methods, however, introduce additional latency due to the sweep operation.

One way to actually synthesize a broader beam is to apply amplitude tapering. In the most extreme case, this reduces to transmission from a single active element [6]. However, since practical transmitters employ a single power amplifier (PA) per antenna, this results in a significant reduction in output power due to poor utilization of power resources. Several amplitude-tapering techniques have been proposed in literature. For instance, a beamforming method proposed in [7] combines a basis pattern with low gain variations over angle and a phase sequence to ensure equal average power in each direction. A numerical method proposed in [8] minimizes the gap with the ideal beam pattern, derived via the Parseval identity, using an iterative multi-convex optimization algorithm. The proposed solution further utilizes the same-beampattern theorem of [9] to loop over a set of designed beamformers, having the same radiation pattern, to select the one that maximizes the PA utilization. An eigenvalue-based optimization approach for codebook beam broadening is proposed in [10]. Another broad beamforming method, based on minimization of the transmit power, is proposed in [11]. Furthermore, in [12], a broad beam is designed by means of Riemannian optimization. Semi-definite programming is applied to broad beam design in [13].

Nevertheless, it is proven in [6] that the *only* solution able to achieve constant array factor for all angles, at a given time instant, is the trivial solution where only one out of all antennas is active. By allowing for a small variation in transmitted power over the angles, the authors of [6] were able to find a set of quasi-broad beamforming vectors where all antennas radiate. Similarly to [8], based on the teachings of [9], an exhaustive search is performed over the set beamformers to obtain the one with maximum PA efficiency. Nevertheless, similarly to the aforementioned algorithms, the obtained solution exhibits mediocre utilization of PAs due to variations in the amplitude of the beamforming vector entries.

A power-efficient alternative to the above methods is to apply phase tapering. That is, optimize the phases of the excitation weights, while keeping their amplitudes fixed. This, however, typically results in a power pattern with significant ripple. For instance, a method based on Zadoff-Chu sequences, proposed in [14], designs beamforming weights that ensure

S. O. Petersson is with Ericsson Research, Gothenburg, Sweden. M. A. Girnyk is with Ericsson Networks, Stockholm, Sweden.

that the signal powers are equal at a set of discrete angles, as many as there are antennas in the array. In [15], a method for beam broadening was proposed by drawing numerous random weight phases and picking the broadest pattern, satisfying certain conditions. Another broadening approach was proposed in [16], where a broadener function is applied to a reference beamforming vector, typically based on a DFT vector. By optimizing parameters of the broadening function, it is possible to increase the angular span of the beam, while reducing the ripple to some acceptable level. Nevertheless, all of the above approaches result in ripple in the shape of the beam.

We note that most of the state-of-the-art references assume that the antenna array is operating with a *single polarization*. However, since the beginning of 4G the majority of antennas, practically used for mobile communications, are *dual-polarized*. That is, an antenna array typically operates with a pair of orthogonal polarizations. Furthermore, most antenna systems are *not* designed with truly omnidirectional coverage in mind. Instead, they are built to cover an angular sector corresponding to a cell [10], [17], [18]. For example, in a conventional three-sector deployment, a cell has the angular width of only 120°.

Considering the above observations, this paper rests on a slightly different problem formulation, where the total transmitted power, i.e., the sum of powers from two orthogonal polarizations, defines the radiation pattern. This novel approach to beamforming, referred to as dual-polarization beamforming, was recently introduced in [19]. Such a formulation allows us to develop a beamforming technique that, as it turns out, makes it possible to find phase-only beamformers that result in total power patterns whose array factor is flat over all angles at any instant in time, with a slightly increased number of design parameters.

Resting on the ideas of [19], this paper proposes a novel technique, referred to as *array-size invariant* (ASI) beamforming, which is based on successive expansion of an antenna array, while preserving its radiation pattern shape. Furthermore, the ASI technique preserves the power utilization of the protoarray without introducing any taper loss. Thus, for instance, if the protoarray is excited with a phase-only weight vector, the expanded array will also have phase-only weights, thereby ensuring excellent power utilization. The technique is applicable to both one- and two-dimensional *uniform antenna* arrays. Finally, it is practically useful since most of the real-world antenna arrays are indeed dual-polarized and hence are able to readily adopt the proposed technique.

The paper's contributions can be summarized as follows:

- We introduce the concept of ASI beamforming which allows one to increase the size of an antenna array, while preserving the total radiation pattern of the original array, as well as ensuring that the power utilization is as efficient for the expanded array as for the original array.
- We propose computationally-efficient algorithms for synthesizing perfectly broad beams (with an array factor without any spatial ripple) for both one- and two-dimensional uniform arrays of arbitrarily large size.
- We showcase the benefits of the proposed ASI beamforming technique by providing several numerical examples: design of a broad beam with flat array factor for uniform linear and rectangular arrays, as well as practical broad beam for public-channel transmission in a realistic network deployment. We show that the proposed beamforming method outperforms existing methods in terms of coverage and energy efficiency.

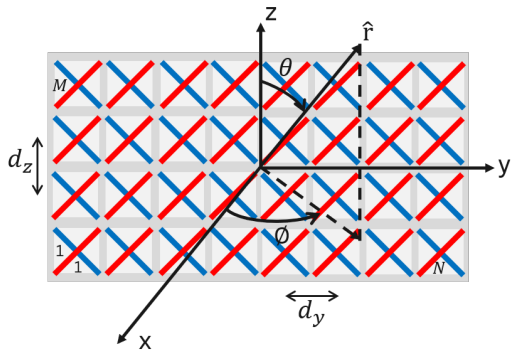

Fig. 1: A dual polarized $M \times N$-element URA.

The remainder of the paper is organized as follows. Sec. II presents the system model, considered antenna array configurations, as well as a review of existing approaches for broad beam generation. Sec. III presents the main results of the paper: methods for generating broad beams for one- and two-dimensional arrays. Sec. IV illustrates the obtained findings by means of numerical examples. Finally, Sec. V presents the conclusions of the study.

The following notations are used throughout the paper. Upper-case and lower-case boldface letters respectively denote matrices and column vectors. Hereafter, $[\cdot]^T$ denotes transpose, $[\cdot]^*$ denotes conjugate, $[\cdot]^H$ denotes Hermitian transpose, $\mathbf{I}_N$ denotes the $N \times N$ identity matrix, and $\mathbf{J}_N$ denotes the $N \times N$ exchange matrix, i.e., a matrix with ones on the anti-diagonal. The Kronecker product of two matrices $\mathbf{A}$ and $\mathbf{B}$ is denoted as $\mathbf{A} \otimes \mathbf{B}$. Vectorization of matrix $\mathbf{A}$ is denoted as $\mathrm{vec}(\mathbf{A})$.

II. System Model and Problem Formulation

The antenna arrays considered in this paper are of two types, uniform linear arrays (ULAs) and uniform rectangular arrays (URAs). It is assumed that all elements in the arrays are identical dual-polarized antenna elements. It is further assumed that the embedded elements are ideal, meaning that the power patterns for the two polarizations are identical and that the element polarizations are perfectly orthogonal. Fig. 1 shows an illustration of a URA $M \times N$-elements, for which element positions, polarizations and element orientation are indicated. The URA collapses into an N-element ULA when we consider the one-dimensional case.

A. Uniform Linear Array

The steering vector $\mathbf{a}(\hat{\mathbf{r}})$ for a ULA reads as

$$\mathbf{a}(\hat{\mathbf{r}}) = [a_1(\hat{\mathbf{r}}), a_2(\hat{\mathbf{r}}), \ldots, a_N(\hat{\mathbf{r}})]^T, \tag{1}$$

where the nth entry is given by

$$a_n(\hat{\mathbf{r}}) = \exp(2\pi j\ \hat{\mathbf{r}}^T \mathbf{p}_n), \tag{2}$$

with $\mathbf{p}_n$ being the position of the nth element, given by

$$\mathbf{p}_n = \left[0,\ \left(n - \frac{N+1}{2}\right) d_{\mathrm{y}},\ 0\right]^T, \tag{3}$$

and $\hat{\mathbf{r}}$ being a direction vector of unit length, defined as

$$\hat{\mathbf{r}} = [\sin\theta\cos\phi,\ \sin\theta\sin\phi,\ \cos\theta]^T, \tag{4}$$

with ϕ being the azimuth angle, θ being the zenith angle and d_{y} being the element spacing in wavelengths along the y-axis.[1]

Modern communication systems are equipped with dual-polarized antennas with almost orthogonal polarizations. Hence, one can design a desired beam as a total power radiation pattern, i.e., the sum of the partial, per polarization, power patterns by means of the *dual-polarization beamforming* (DPBF) technique [19]. Remarkably, the DPBF beamformer proposed in [19] is constant-modulus, thereby having much more efficient use of the available output power than that of single-polarization beamformers.

Looking at the total radiated power rather than the radiated power for a given polarization—the conventional approach in the beamforming literature—means that the polarization of the transmitted signal is actually not taken into account. At first, this might seem counter-intuitive, however, it can be justified by the polarization at the user equipment (UE) being anyway unknown in practice. The latter is due to the impact of the radio channel, the unknown orientation of the UE and the unknown polarization of the UE antenna(s). To counteract performance losses due to all these effects, diversity reception has become a conventional operation at the receive end. Furthermore, if desired, there is always a possibility to create a second beam with identical total power pattern and orthogonal polarization in all directions.

The total complex electric field radiated by the array, when excited by beamforming weight vectors $\mathbf{w}_{\mathrm{A}}$, for polarization A, and $\mathbf{w}_{\mathrm{B}}$, for polarization B, is given by

$$\mathbf{e}(\hat{\mathbf{r}}) = \begin{bmatrix} \mathrm{e}_{\mathrm{A}}(\hat{\mathbf{r}}) \\ \mathrm{e}_{\mathrm{B}}(\hat{\mathbf{r}}) \end{bmatrix} = \begin{bmatrix} \mathbf{w}_{\mathrm{A}}^T \mathbf{a}(\hat{\mathbf{r}}) \\ \mathbf{w}_{\mathrm{B}}^T \mathbf{a}(\hat{\mathbf{r}}) \end{bmatrix} E_{\mathrm{el}}(\hat{\mathbf{r}}), \tag{5}$$

where $E_{\mathrm{el}}(\hat{\mathbf{r}})$ is the electric field radiated by a single antenna element, identical for both polarizations.

The total power radiation pattern is found by superposition of the power for the orthogonal polarizations as

$$G(\hat{\mathbf{r}}) = \mathbf{e}(\hat{\mathbf{r}})^H\ \mathbf{e}(\hat{\mathbf{r}}) \tag{6}$$

$$= A(\hat{\mathbf{r}}) G_{\mathrm{el}}(\hat{\mathbf{r}}), \tag{7}$$

where $G_{\mathrm{el}}(\hat{\mathbf{r}}) = |E_{\mathrm{el}}(\hat{\mathbf{r}})|^2$ is the element power pattern and $A(\hat{\mathbf{r}})$ is the array factor. As DPBF involves a sum over two orthogonal polarizations, the conventional definition of array factor does not apply. Instead, the latter is defined as

$$A(\hat{\mathbf{r}}) = \mathbf{a}(\hat{\mathbf{r}})^H (\mathbf{w}_{\mathrm{A}}{}^* \mathbf{w}_{\mathrm{A}}{}^T + \mathbf{w}_{\mathrm{B}}{}^* \mathbf{w}_{\mathrm{B}}{}^T)\ \mathbf{a}(\hat{\mathbf{r}}). \tag{8}$$

[1]Note that we here have defined the ULA as a horizontal array to address the issue of forming broad beams in azimuth. This may be useful in the cases where one needs to cover an entire sector with broadcast information. Nevertheless, the need for broad beams also exists in the elevation domain, e.g., to cover a high-rise building.

B. Uniform Rectangular Array

Similarly to the case of ULA, the (m,n)th entry in the steering matrix $\mathbf{A}(\hat{\mathbf{r}})$ for a URA reads

$$a_{m,n}(\hat{\mathbf{r}}) = \exp(2\pi j\ \hat{\mathbf{r}}^T \mathbf{p}_{m,n}), \tag{9}$$

where the position of the (m,n)th element is given by

$$\mathbf{p}_{m,n} = \left[0,\ \left(n - \frac{N+1}{2}\right) d_{\mathrm{y}},\ \left(m - \frac{M+1}{2}\right) d_{\mathrm{z}}\right]^T, \tag{10}$$

with d_{z} being the element spacing in wavelengths along the z-axis.

The total complex far-field pattern is found, in a similar way as for the ULA, when excited by beamforming matrices $\mathbf{W}_{\mathrm{A}}$, for polarization A, and $\mathbf{W}_{\mathrm{B}}$, for polarization B, as

$$\mathbf{e}(\hat{\mathbf{r}}) = \begin{bmatrix} \mathrm{vec}^T(\mathbf{W}_{\mathrm{A}})\,\mathrm{vec}(\mathbf{A}(\hat{\mathbf{r}})) \\ \mathrm{vec}^T(\mathbf{W}_{\mathrm{B}})\,\mathrm{vec}(\mathbf{A}(\hat{\mathbf{r}})) \end{bmatrix} E_{\mathrm{el}}(\hat{\mathbf{r}}). \tag{11}$$

The total power radiation pattern is, as for the ULA, found by superposition of the power for the orthogonal polarizations, as in (7). The array factor definition for a URA is similar to that for a ULA, and it is given by

$$A(\hat{\mathbf{r}}) = \mathrm{vec}(\mathbf{A}(\hat{\mathbf{r}}))^H \left[\mathrm{vec}^*(\mathbf{W}_{\mathrm{A}})\mathrm{vec}^T(\mathbf{W}_{\mathrm{A}}) + \mathrm{vec}^*(\mathbf{W}_{\mathrm{B}})\mathrm{vec}^T(\mathbf{W}_{\mathrm{B}})\right] \mathrm{vec}(\mathbf{A}(\hat{\mathbf{r}})). \tag{12}$$

C. Broad Beam Concept

In this paper, a *broad beam* is referred to as a radiation pattern with limited variation in total radiated power in all directions within an angular sector of interest. A beamforming method that produces such a beam shape shall allow for the following:

- Creating a desired power pattern (for example, but not limited to, the power pattern of a single element);
- Using the distributed power resource in an efficient way (ideally by having constant modulus beamforming weights).

As an extreme case of the above requirements, a broad beam could be defined as the total power radiation pattern, in (7), being identical to the power radiation pattern of a single element. Equivalently, the array factor must be flat, i.e.,

$$A(\hat{\mathbf{r}}) = c, \tag{13}$$

for any direction $\hat{\mathbf{r}}$, where c is a constant.

D. Existing Approaches

As mentioned in Sec. I, the subject of finding beamformers that fulfill (13) has received some scholarly attention over the years. Common to all the prior research is an assumption that beamforming is performed using an array where all elements are identical, with respect to both radiation pattern and polarization, i.e., *single-polarization beamforming* (SPBF). Amplitude and phase tapering are widely used approaches for designing a beam with spatially flat array factor for such arrays [6], [16].

With amplitude tapering one can optimize amplitudes and phases of the excitation weights to produce a broad beam shape. Unfortunately, as proven in [6], the only true solution for the problem of designing such a broad beam by means of SPBF is the trivial one where only one element in the excitation vector is active. This solution is, however, not acceptable in the case of active antennas due to the poor utilization of the available power resources in the antenna array, especially in massive MIMO deployments. Another common method for designing a broad beam with improved power utilization is phase tapering. In this case, the corresponding algorithm optimizes only phases of the excitation weights, while keeping the amplitudes constant. In this way, it ensures the all the available power is utilized. There is, however, a limit to the extent to which phase tapering can achieve a broad target beam shape. Typically, it leads to a certain unavoidable amount of ripple in the power pattern.

As spotted in [20], there is a trade-off between power utilization and beam ripple achievable using amplitude and phase tapering. Yet another possible approach is to address this trade-off by means of multi-objective optimization [21]. Such a solution provides a compromise between the two requirements: constant beam shape and efficient power utilization.

III. Array-Size Invariant Beamforming

Although providing practically acceptable means for wide-sector coverage, existing SPBF solutions do not enable the generation of broad beams with a flat array factor. In this section, we introduce the concept of *array-size invariant* (ASI) beamforming that provides a means for generating broad beams of controllable width. The concept is based on the previously reported technique of creating beams with identical power patterns and orthogonal polarizations by means of DPBF [19]. The main idea is to utilize the additional degree of freedom that comes from using orthogonal polarizations when designing the antenna excitation weights resulting in a desired beam shape. The excitation weights can often be designed with no amplitude taper leading to full power utilization.

The central technique of the ASI approach is the successive doubling of the size of the array while preserving its power radiation pattern, which we refer to as the *expansion technique*. Consider, for instance, a ULA with N dual-polarized antennas which has been designed so that its power radiation pattern has a desired shape (e.g., as broad as the pattern of a single element); we refer to such an array as a *protoarray*. The task of the expansion technique is to expand the protoarray into an *expanded array* of a larger size, while preserving the radiation pattern of the former. This is done by designing a second array that would be appended to the protoarray without distorting the resulting power pattern; this second array is referred to as the *companion array*, and it has the same geometry as the protoarray. By appending the companion array to the protoarray, we get an expanded array of size $2N$ with the same power radiation pattern as the former.

1) ULA expansion: Consider a protoarray of size N, excited with beamforming weights $\mathbf{w}_{1,\mathrm{A}}$ and $\mathbf{w}_{1,\mathrm{B}}$ for the respective polarizations. In order to expand it, while preserving the radiation pattern, the conditions of the following proposition should hold.

Proposition 1. *Let $(\mathbf{w}_{1,\mathrm{A}}, \mathbf{w}_{1,\mathrm{B}})$ be a pair of per-polarization excitation vectors applied to a protoarray yielding a desired beam shape. Let, furthermore, $(\mathbf{w}_{2,\mathrm{A}}, \mathbf{w}_{2,\mathrm{B}})$ be a pair of per-polarization excitation vectors applied to a companion array appended to the protoarray. The radiation pattern of the expanded array with per-polarization weights given by*

$$\mathbf{w}_{\mathrm{A}} = [\mathbf{w}_{1,\mathrm{A}}^T, \mathbf{w}_{2,\mathrm{A}}^T]^T, \tag{14}$$

$$\mathbf{w}_{\mathrm{B}} = [\mathbf{w}_{1,\mathrm{B}}^T, \mathbf{w}_{2,\mathrm{B}}^T]^T, \tag{15}$$

preserves the shape of the pattern of the protoarray if

$$\mathbf{w}_{2,\mathrm{A}} = -\mathbf{J}_N \mathbf{w}_{1,\mathrm{B}}^*, \tag{16}$$

$$\mathbf{w}_{2,\mathrm{B}} = \mathbf{J}_N \mathbf{w}_{1,\mathrm{A}}^*. \tag{17}$$

Proof: First, we note that the radiation pattern of the protoarray is given by

$$G_1(\hat{\mathbf{r}}) = \left[|\mathbf{w}_{1,\mathrm{A}}^T \mathbf{a}_1(\hat{\mathbf{r}})|^2 + |\mathbf{w}_{1,\mathrm{B}}^T \mathbf{a}_1(\hat{\mathbf{r}})|^2\right] G_{\mathrm{el}}(\hat{\mathbf{r}}). \tag{18}$$

After appending the companion array to the protoarray, we obtain an expanded array of size $2N$ with excitation weights given by (14) and (15), as well as the steering vector given by

$$\mathbf{a}(\hat{\mathbf{r}}) = [a_1(\hat{\mathbf{r}}), \cdots, a_{2N}(\hat{\mathbf{r}})]^T. \tag{19}$$

The radiated electric-field vector of the expanded array is given by the superposition of the fields of the two parts, i.e.,

$$\mathbf{e}(\hat{\mathbf{r}}) = \mathbf{e}_1(\hat{\mathbf{r}}) + \mathbf{e}_2(\hat{\mathbf{r}}) \tag{20}$$

$$= \begin{bmatrix} \mathbf{w}_{1,\mathrm{A}}^T \mathbf{a}_1(\hat{\mathbf{r}}) + \mathbf{w}_{2,\mathrm{A}}^T \mathbf{a}_2(\hat{\mathbf{r}}) \\ \mathbf{w}_{1,\mathrm{B}}^T \mathbf{a}_1(\hat{\mathbf{r}}) + \mathbf{w}_{2,\mathrm{B}}^T \mathbf{a}_2(\hat{\mathbf{r}}) \end{bmatrix} E_{\mathrm{el}}(\hat{\mathbf{r}}). \tag{21}$$

The total radiation power pattern of the expanded array is thus given by

$$G(\hat{\mathbf{r}}) = \mathbf{e}^H(\hat{\mathbf{r}}) \mathbf{e}(\hat{\mathbf{r}}) \tag{22}$$

$$= \|\mathbf{e}_1(\hat{\mathbf{r}})\|^2 + \|\mathbf{e}_2(\hat{\mathbf{r}})\|^2 + 2\,\mathrm{Re}\left\{\mathbf{e}_1^H(\hat{\mathbf{r}}) \mathbf{e}_2(\hat{\mathbf{r}})\right\}. \tag{23}$$

If the electric field vectors radiated from the two subarrays are orthogonal, the last term disappears. Consider the product

$$\mathbf{e}_1^H(\hat{\mathbf{r}})\, \mathbf{e}_2(\hat{\mathbf{r}}) = \left[\mathbf{a}_1^H(\hat{\mathbf{r}}) \mathbf{w}_{1,\mathrm{A}}^* \mathbf{w}_{2,\mathrm{A}}^T \mathbf{a}_2(\hat{\mathbf{r}}) + \mathbf{a}_1^H(\hat{\mathbf{r}}) \mathbf{w}_{1,\mathrm{B}}^* \mathbf{w}_{2,\mathrm{B}}^T \mathbf{a}_2(\hat{\mathbf{r}})\right] G_{\mathrm{el}}(\hat{\mathbf{r}}). \tag{24}$$

We notice that the steering vectors of the companion array and the protoarray are related as

$$\mathbf{a}_2(\hat{\mathbf{r}}) = e^{jN\psi_{\mathrm{y}}}\, \mathbf{a}_1(\hat{\mathbf{r}}), \tag{25}$$

where $\psi_{\mathrm{y}} = -2\pi d_{\mathrm{y}} \sin\theta \sin\phi$. Next, we plug in the weights given in (16) and (17) and, utilizing the fact that

$$\mathbf{J}_N \mathbf{a}_1(\hat{\mathbf{r}}) = e^{j(N-1)\psi_{\mathrm{y}}}\, \mathbf{a}_1^*(\hat{\mathbf{r}}), \tag{26}$$

as well as transposing the second term, we get

$$\mathbf{e}_1^H(\hat{\mathbf{r}})\, \mathbf{e}_2(\hat{\mathbf{r}}) = \left[-\mathbf{a}_1^H(\hat{\mathbf{r}}) \mathbf{w}_{1,\mathrm{A}}^* \mathbf{w}_{1,\mathrm{B}}^H \mathbf{a}_1^*(\hat{\mathbf{r}}) e^{j(2N-1)\psi_{\mathrm{y}}} + \left(\mathbf{a}_1^H(\hat{\mathbf{r}}) \mathbf{w}_{1,\mathrm{A}}^* \mathbf{w}_{1,\mathrm{B}}^H \mathbf{a}_1^*(\hat{\mathbf{r}}) e^{j(2N-1)\psi_{\mathrm{y}}}\right)^T\right] G_{\mathrm{el}}(\hat{\mathbf{r}}). \tag{27}$$

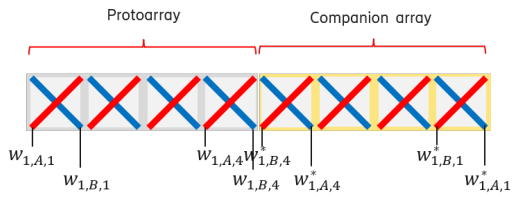

Fig. 2: Array expansion of a ULA by appending a synthesized companion array to the protoarray.

Since both summands are scalars, the transposition operation does not affect them, and hence the two terms inside the braces cancel each other out, yielding $\mathbf{e}_1^H(\hat{\mathbf{r}})\mathbf{e}_2(\hat{\mathbf{r}}) = 0$. Thus, the choice of beamforming weights for the companion array in (16) and (17) leads to the two electric fields being orthogonal for every observation angle. The total power radiation pattern is therefore given by

$$G(\hat{\mathbf{r}}) = 2\left[|\mathbf{w}_{1,\mathrm{A}}^T\mathbf{a}_1(\hat{\mathbf{r}})|^2 + |\mathbf{w}_{1,\mathrm{B}}^T\mathbf{a}_1(\hat{\mathbf{r}})|^2\right] G_{\mathrm{el}}(\hat{\mathbf{r}}) \tag{28}$$

$$= 2\, G_1(\hat{\mathbf{r}}), \tag{29}$$

being a scaled version of the pattern of the protoarray (18). ■

The procedure described above is illustrated in Fig. 2. A companion array whose weights are chosen according to (16) and (17) is attached to the protoarray, ensuring that the expanded array preserves the beam shape of the latter. Note that by choosing the beamforming weights for the companion array as in (16) and (17), one makes the electric fields radiated by the two subarrays *orthogonal* regardless of the observation angle. As a result, the corresponding beams add up incoherently (i.e., power addition) and the resulting radiation pattern of the entire expanded array does not shrink.

The above procedure can be conducted successively k times to obtain a k-fold array expansion summarized in Algorithm 1. Remarkably, if the expansion starts from a single antenna element, the entire array will have an array pattern that is a scaled version of the pattern of an individual element. At the same time, all the PAs of the expanded array are fully utilized, and, in principle, there exists no upper limit for the size of such an expanded array.

It is worth noticing that the power utilization, or in other words taper loss, of the expanded array is the same as that of the protoarray. Thus, it is important to design the protoarray to have low taper loss. Furthermore, another benefit of the ASI beamforming is that the degrees of freedom, which are given by the size of the protoarray, are reduced, simplifying the optimization of the beamforming weights.

2) URA expansion: Consider a rectangular protoarray of size $N \times M$, excited with beamforming weights $\mathbf{W}_{1,\mathrm{A}}$ and $\mathbf{W}_{1,\mathrm{B}}$ for the respective polarizations. In order to expand it while preserving the shape of the total power radiation pattern, the conditions of the following proposition should hold.

Proposition 2. *Let* $(\mathbf{W}_{1,\mathrm{A}}, \mathbf{W}_{1,\mathrm{B}})$ *be a pair of per-polarization excitation matrices applied to a protoarray yielding a desired beam shape. Let, furthermore,* $(\mathbf{W}_{2,\mathrm{A}}, \mathbf{W}_{2,\mathrm{B}})$ *be a pair of per-polarization excitation matrices applied to a companion array appended to the protoarray. The radiation pattern of the expanded array with per-polarization weights given by one of the ways below,*

$$\mathbf{W}_{\mathrm{A}} = [\mathbf{W}_{1,\mathrm{A}}^T, \mathbf{W}_{2,\mathrm{A}}^T]^T, \quad \mathbf{W}_{\mathrm{B}} = [\mathbf{W}_{1,\mathrm{B}}^T, \mathbf{W}_{2,\mathrm{B}}^T]^T, \tag{30}$$

$$\mathbf{W}_{\mathrm{A}} = [\mathbf{W}_{1,\mathrm{A}}, \mathbf{W}_{2,\mathrm{A}}], \quad \mathbf{W}_{\mathrm{B}} = [\mathbf{W}_{1,\mathrm{B}}, \mathbf{W}_{2,\mathrm{B}}], \tag{31}$$

preserves the shape of the pattern of the protoarray if the companion array is excited with

$$\mathbf{W}_{2,\mathrm{A}} = -\mathbf{J}_M\mathbf{W}_{1,\mathrm{B}}^*\mathbf{J}_N, \tag{32}$$

$$\mathbf{W}_{2,\mathrm{B}} = \mathbf{J}_M\mathbf{W}_{1,\mathrm{A}}^*\mathbf{J}_N. \tag{33}$$

Algorithm 1 ULA Expansion.

Require: Size $K = 2^kN$ of the desired large array, N-antenna protoarray with a pre-designed pattern given by weights $\mathbf{w}_{1,A}$ and $\mathbf{w}_{1,B}$.

1: **for** $i \leftarrow 1$ to k **do**
2: Compute the excitation weight vectors $\mathbf{w}_{2,A}$ and $\mathbf{w}_{2,B}$ of the companion array using (16) and (17).
3: Stack the weight vectors of the companion array and the protoarray as in (14) and (15) and obtain the excitation weight vectors $\mathbf{w}_A$ and $\mathbf{w}_B$ of the expanded array.
4: $(\mathbf{w}_{1,A}, \mathbf{w}_{1,B}) \leftarrow (\mathbf{w}_A, \mathbf{w}_B)$, i.e., replace the protoarray with the expanded array.
5: **end for**

Proof: Here we follow the same steps as in the case of ULA. The radiated electric-field vector of the expanded array is given by the superposition of the fields of the two parts,

$$\mathbf{e}(\hat{\mathbf{r}}) = \mathbf{e}_1(\hat{\mathbf{r}}) + \mathbf{e}_2(\hat{\mathbf{r}}), \tag{34}$$

and the total power pattern of the expanded array reads as

$$G(\hat{\mathbf{r}}) = \|\mathbf{e}_1(\hat{\mathbf{r}})\|^2 + \|\mathbf{e}_2(\hat{\mathbf{r}})\|^2 + 2\,\mathrm{Re}\left\{\mathbf{e}_1^H(\hat{\mathbf{r}})\mathbf{e}_2(\hat{\mathbf{r}})\right\}. \tag{35}$$

The last term disappears when

$$\mathrm{vec}^H(\mathbf{A}_1(\hat{\mathbf{r}}))\mathrm{vec}^*(\mathbf{W}_{1,\mathrm{A}})\mathrm{vec}^T(\mathbf{W}_{2,\mathrm{A}})\mathrm{vec}(\mathbf{A}_2(\hat{\mathbf{r}})) + \mathrm{vec}^H(\mathbf{A}_1(\hat{\mathbf{r}}))\mathrm{vec}^*(\mathbf{W}_{1,\mathrm{B}})\mathrm{vec}^T(\mathbf{W}_{2,\mathrm{B}})\mathrm{vec}(\mathbf{A}_2(\hat{\mathbf{r}})) = 0. \tag{36}$$

We notice that the steering matrices of the companion array and the protoarray are related as

$$\mathbf{A}_2(\hat{\mathbf{r}}) = \kappa\mathbf{A}_1(\hat{\mathbf{r}}), \tag{37}$$

where $\kappa = \exp(jN\psi_{\mathrm{z}})$, with $\psi_{\mathrm{z}} = -2\pi d_{\mathrm{z}}\cos\theta$, when the companion array is attached as in (30), and $\kappa = \exp(jM\psi_{\mathrm{y}})$, with $\psi_{\mathrm{y}} = -2\pi d_{\mathrm{y}}\sin\theta\sin\phi$, when it is attached as in (31). We plug in the excitation weights given in (32) and (33) and, utilizing the fact that

$$\mathbf{J}_M\mathbf{A}_1(\hat{\mathbf{r}})\mathbf{J}_N = \xi\mathbf{A}_1^*(\hat{\mathbf{r}}), \tag{38}$$

where $\xi = \exp(j\,[(N-1)\psi_{\mathrm{y}} + (M-1)\psi_{\mathrm{z}}])$, and, transposing the second term, we see that

$$-\mathrm{vec}^H(\mathbf{A}_1(\hat{\mathbf{r}}))\mathrm{vec}^*(\mathbf{W}_{1,\mathrm{A}})\mathrm{vec}^H(\mathbf{W}_{1,\mathrm{B}})\mathrm{vec}^*(\mathbf{A}_1(\hat{\mathbf{r}}))\kappa\xi + (\mathrm{vec}^H(\mathbf{A}_1(\hat{\mathbf{r}}))\mathrm{vec}^*(\mathbf{W}_{1,\mathrm{A}})\mathrm{vec}^H(\mathbf{W}_{1,\mathrm{B}})\mathrm{vec}^*(\mathbf{A}_1(\hat{\mathbf{r}}))\kappa\xi)^T = 0, \tag{39}$$

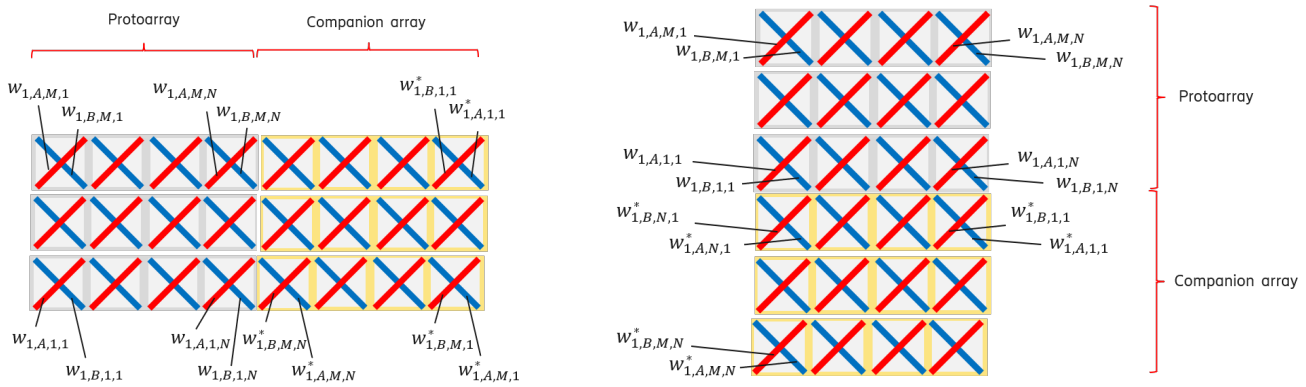

(a) Horizontal expansion. (b) Vertical expansion.

Fig. 3: Array expansion of a URA by appending the companion array to the protoarray in different ways.

since both summands are scalars. Therefore, $\mathbf{e}_1^H(\hat{\mathbf{r}})\mathbf{e}_2(\hat{\mathbf{r}}) = 0$, and the choice of weights for the companion array in (32) and (33) leads to the electric fields generated by the two subarrays being orthogonal for every angle. The total radiation power pattern of the expanded array is thus given by

$$G(\hat{\mathbf{r}}) = 2\left[|\mathrm{vec}^T(\mathbf{W}_{1,\mathrm{A}})\mathrm{vec}(\mathbf{A}(\hat{\mathbf{r}})|^2 + |\mathrm{vec}^T(\mathbf{W}_{1,\mathrm{B}})\mathrm{vec}(\mathbf{A}(\hat{\mathbf{r}})|^2\right] G_{\mathrm{el}}(\hat{\mathbf{r}}) \quad (40)$$

$$= 2\, G_1(\hat{\mathbf{r}}), \quad (41)$$

being a scaled version of the pattern of the protoarray. ■

The procedure is illustrated in Fig. 3 on the top of the next page. Similarly to the one-dimensional case, the expansion can also be repeated successively $k + l$ times to produce an expanded URA that preserves the radiation pattern of its protoarray, as summarized in Algorithm 2.

Note that in the two-dimensional setting, the companion array can be appended in various ways: horizontally, vertically, etc. Interestingly, the order of expansion—horizontal, then vertical, or vice versa—does not influence the final radiation pattern, as far as total power pattern is concerned. The important requirement is that the protoarray and the companion array have the same geometry in each iteration.

Algorithm 2 URA Expansion.

Require: Size $L \times K$ of the desired large array, where $L = 2^l M$ and $K = 2^k N$, $M \times N$-antenna protoarray with a pre-designed pattern via per-polarization weight matrices $\mathbf{W}_{1,A}$ and $\mathbf{W}_{1,B}$.

`// Horizontal expansion`

for $j \leftarrow 1$ to k **do**
  Compute the excitation weight matrices $\mathbf{W}_{2,A}$ and $\mathbf{W}_{2,B}$ of the companion array using (32) or (33).
  Stack the weight matrices of the companion array and the protoarray as in (30), and obtain the excitation weight matrices $\mathbf{W}_A$ and $\mathbf{W}_B$ of an expanded array.
  $(\mathbf{W}_{1,A}, \mathbf{W}_{1,B}) \leftarrow (\mathbf{W}_A, \mathbf{W}_B)$, i.e., replace the protoarray with the expanded array.
end for

`// Vertical expansion`

for $i \leftarrow 1$ to l **do**
  Compute the excitation weight matrices $\mathbf{W}_{2,A}$ and $\mathbf{W}_{2,B}$ of the companion array using (32) or (33).
  Stack the weight matrices of the companion array and the protoarray as in (30), and obtain the excitation weight matrices $\mathbf{W}_A$ and $\mathbf{W}_B$ of an expanded array.
  $(\mathbf{W}_{1,A}, \mathbf{W}_{1,B}) \leftarrow (\mathbf{W}_A, \mathbf{W}_B)$, i.e., replace the protoarray with the expanded array.
end for

IV. Numerical Results

In the previous section, we have shown that by means of the ASI technique it is possible to, for many array sizes, design a beamformer that not only results in a desired total power pattern, but also ensures very efficient utilization of PAs. The companion array, designed according to Algorithms 1 and 2, will have the same power utilization as the protoarray. Therefore, the power utilization for the weights, after expansion, will be the same as that for the protoarray. And, given that each antenna element is fed by identical PAs no matter the size of the array, it follows that the total output power increases by a factor of two for each iteration of the algorithm as the array size increases.

Below, we present several numerical examples illustrating the usefulness of the proposed beamforming method.

A. Spatially Flat Array Factor

One example which has received a lot of interest in literature in recent years is the design of a constant-modulus beamforming vector whose radiation pattern looks like if it was formed by a single antenna element [13], [6]. We recall that a beam pattern of a ULA can be written as a product of the array factor and the element pattern. Hence, for the case where the target is a beam pattern similar to that of a single element, we need to find a spatially flat array factor. Interestingly, this array factor can be found for any ULA, regardless of the element separation. Here we demonstrate how beamforming weights can be designed with a simple example.

For that matter, we set the target to be the power pattern formed by a single element. That is, the protoarray is chosen

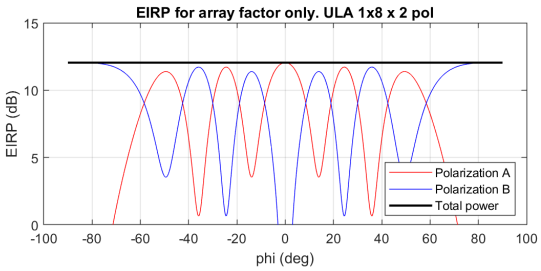

(a) $k = 3$.

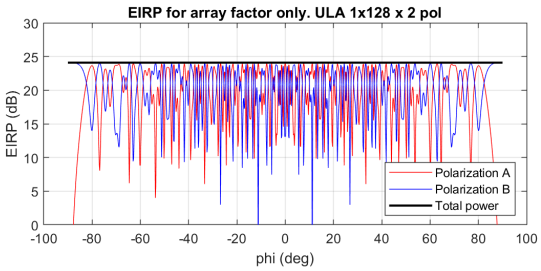

(b) $k = 7$.

Fig. 4: Array factor of a single element after k-fold one-dimensional expansion.

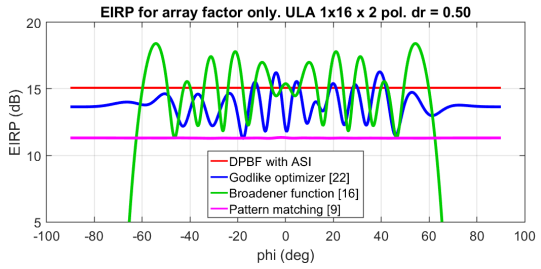

(a) $d_{\mathrm{y}} = 0.5$.

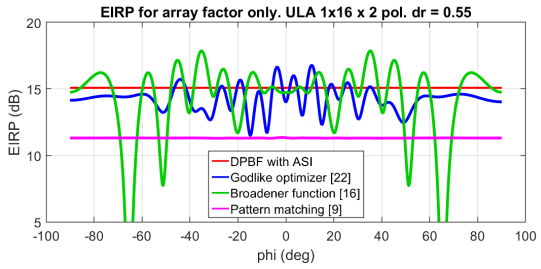

(b) $d_{\mathrm{y}} = 0.55$.

Fig. 5: Optimized array factors: proposed ASI method vs. existing approaches for various element spacings d_{y}.

to be a single dual-polarized element with excitation weights given by, e.g.,

$$\mathbf{w}_{1,\mathrm{A}} = \mathbf{w}_{1,\mathrm{B}} = 1. \tag{42}$$

1) Uniform linear array: Consider a ULA with $N = 8$ dual-polarized antennas. Following the procedure outlined in Algorithm 1, we start with a single element, and expand it $k = 3$ times. As a result, we arrive at a pair of excitation vectors of length $2^k = 8$, each for its corresponding polarization:

$$\mathbf{w}_{\mathrm{A}} = [\,1, -1, -1, -1, -1, \quad 1, -1, -1]^T, \tag{43}$$

$$\mathbf{w}_{\mathrm{B}} = [\,1, \quad 1, -1, \quad 1, -1, -1, -1, \quad 1]^T. \tag{44}$$

As can be seen, these excitation vectors are constant modulus so PAs in an active antenna array can be efficiently utilized with no loss due to amplitude taper.

The array factor corresponding to the excitation weights above is shown in Fig. 4a. As can be seen from the figure, the patterns in individual polarizations fluctuate with spatial angle. However, in every direction, the power of the two orthogonal polarizations adds up to the same value. Thus, the array factor for the total power is flat.

A similar example but for a much larger ULA, now with $N = 128$ elements is shown in Fig. 4b. The beamforming weights were found by means of Algorithm 1 with $k = 7$-fold expansion of a single element. The beamforming vectors are omitted here due to their length. Just as in the previous case, the beamforming vectors are characterized with constant modulus. Therefore, the power loss of more than 8 dB due to amplitude taper, reported in [6] for $N = 128$, can be avoided with the technique proposed herein.

To show the gains of the proposed method, we compare its performance with that of relevant state-of-the-art methods on the task of designing a beam with flat array factor. For the proposed ASI method, the beamforming weights are obtained by expanding the vectors in (43) once by means of (14) – (17).

The first existing alternative approach to compare against is the *pattern-matching* (PM) beamforming [9]. The method optimizes the phases and amplitudes of the weights to match a target beam pattern (see Appendix A for the details). Note that for the task of finding an SPBF beam with flat array factor, the PM method reduces to the approach of [6].

As a more power-efficient alternative, we examine a phase-only beamforming method that modifies a base DFT beamformer with a *broadener function* (BF) [16]. The beamforming weights are optimized by sweeping the broadener parameters (see Appendix B for more on this). The method might not be able to find a flat array factor in the entire angular range; therefore, to make the optimization feasible, we restrict the requirement of flatness to the interval $[-60°, 60°]$.

As a compromise between the previous two methods, we also add weights found by the *Godlike optimizer* (GO) [22] to the comparison. The GO method is a multi-objective optimization algorithm that runs in parallel several optimization jobs, interchanging their solutions after convergence and thereby improving the likelihood of convergence to the global optimum (see Appendix C for more details). We define two objectives for the GO method to minimize: variance of the array factor within the focus interval $[-60°, 60°]$ and PA efficiency measured by the taper loss:

$$L_{\mathrm{taper}}(\mathbf{w}_{\mathrm{A}}, \mathbf{w}_{\mathrm{B}}) = \frac{2N \max\{|[\mathbf{w}_{\mathrm{A}}^T, \mathbf{w}_{\mathrm{B}}^T]^T|^2\}}{\|\mathbf{w}_{\mathrm{A}}\|^2 + \|\mathbf{w}_{\mathrm{B}}\|^2}. \tag{45}$$

Fig. 5 shows the array factor for a ULA with $N = 16$ elements. Note that the patterns are plotted in terms of *equivalent isotropically radiated power* (EIRP). For these plots, the

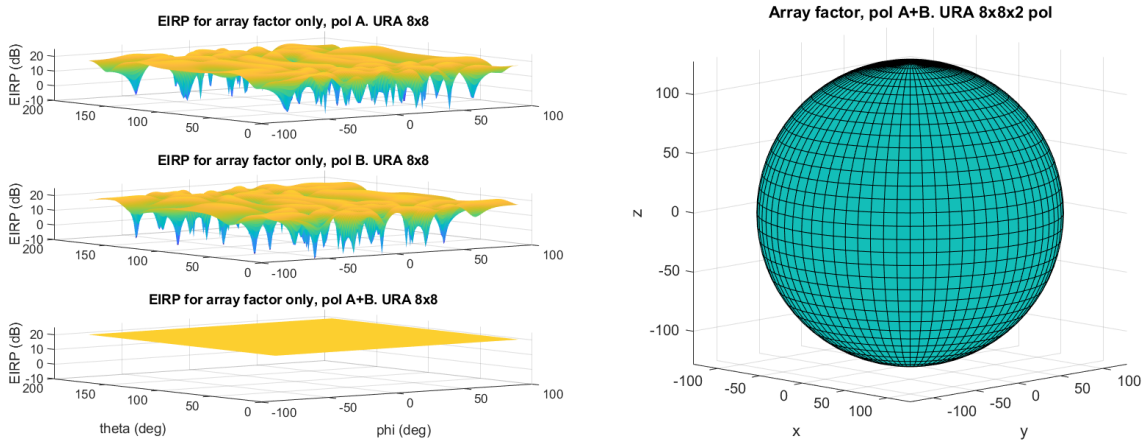

(a) Per-polarization array factors and total array factor.

(b) Total array factor in polar coordinates.

Fig. 6: Array factor of a single element after two-dimensional expansion by a factor of $k = 3$ along each dimension.

beamforming weights are normalized, such that the total output power for both polarizations is 1 W per PA minus taper loss.

The optimized weights for state-of-the-art approaches are summarized in Table I. It can be seen from the figure that the proposed method is able to achieve a perfectly flat array factor, while ensuring transmission from all antennas simultaneously and thereby having excellent PA utilization. Meanwhile, the PM approach, even though being able to achieve a flat array factor, leads to a power loss (~ 3.7 dB for the given array size) due to amplitude variation across antennas. Moreover, the BF approach, albeit having full PA utilization, is characterized by a significant amount of ripple in the array factor even within the chosen angular range (with variance of 3.6 dB in the interval of $[-60°, 60°]$). Finally, the GO method is able to find an array factor with less ripple than the that of the BF solution (variance of 1.3 dB in the aforementioned angular interval), while having reasonably small taper loss (1.1 dB, i.e., less than that of the PM method). Nevertheless, it is clear from the figure that none of the state-of-the-art methods is able to accomplish what is achieved by the proposed ASI method: ripple-free flat array factor in the entire angular range with full PA utilization.

An interesting observation from Fig. 5a is that beamformer generated using the BF method has a null at a certain angle. This is due to the symmetry of the beam pattern coming from the base DFT beam pointing at $\phi = 0°$. The direction of the null depends on the element separation, and it is $\phi = 90°$ for $d_{\mathrm{y}} = 0.5$. In Fig. 5b, we plot the array factors for $d_{\mathrm{y}} = 0.55$ (note that the weights were re-optimized for this spacing), and it is clearly seen that the null appears at smaller values of ϕ. If the base DFT beam would point to a different direction (than at $\phi = 0°$), the nulls would appear at other angles, however there would still be one or more nulls for the BF method. Meanwhile, it is seen from Fig. 6 that ASI, GO and PM methods do not exhibit deep nulls, and are less susceptible to a change in antenna separation d_{y}.

2) Uniform rectangular array: Here we demonstrate that the proposed method is equally applicable to URAs for designing a flat array factor. Consider a URA with $M \times N = 8 \times 8$ antennas. To design the excitation vectors for this case we follow the procedure outlined in Algorithm 2. We start by expanding the single-element protoarray along one dimension. Which dimension to start with does not really matter, but here we have selected to start the expansion along elevation (index j) until we have a one-dimensional array of size 8×1. The excitation vectors after this step, which are identical to the excitation vectors in (43) and (44), now form a new protoarray, which we further expand along the other dimension, i.e., azimuth (index i), to form a two-dimensional array of size 8×8. The resulting excitation weight matrices (one per polarization) are shown in (46) on the top of the page. As can be seen, similarly to the previous case, the excitation matrices are constant-modulus. The array factors per polarization, as well as for total power, are shown in Fig. 6a. The total power array factor is also shown in Fig. 6b in polar coordinates. As can be seen from Fig. 6, the array factor for total power is spatially flat and thus the resulting power radiation pattern will be a scaled version of the element pattern.

TABLE I: Beamforming weight vectors optimized to obtain a flat array factor.

GO method	BF method	PM method
$0.014 - 0.170j$	$-0.118 - 0.132j$	$-0.002 - 0.005j$
$0.049 - 0.134j$	$0.175 + 0.028j$	$-0.025 - 0.001j$
$-0.121 + 0.068j$	$0.138 + 0.110j$	$-0.038 + 0.042j$
$-0.110 - 0.063j$	$0.026 - 0.175j$	$-0.002 + 0.103j$
$-0.250 - 0.174j$	$0.154 - 0.086j$	$0.104 + 0.111j$
$-0.060 - 0.166j$	$-0.163 + 0.069j$	$0.167 + 0.005j$
$-0.084 + 0.155j$	$0.034 + 0.173j$	$0.045 - 0.096j$
$-0.168 + 0.056j$	$0.093 + 0.150j$	$-0.022 + 0.115j$
$0.174 - 0.030j$	$0.093 + 0.150j$	$0.174 + 0.000j$
$-0.165 - 0.064j$	$0.034 + 0.173j$	$-0.083 + 0.058j$
$0.148 - 0.097j$	$-0.163 + 0.069j$	$0.091 + 0.057j$
$0.057 - 0.167j$	$0.154 - 0.086j$	$-0.126 + 0.124j$
$-0.042 + 0.118j$	$0.026 - 0.175j$	$-0.104 - 0.121j$
$0.096 + 0.031j$	$0.138 + 0.110j$	$0.075 - 0.062j$
$0.023 + 0.126j$	$0.175 + 0.028j$	$0.028 + 0.036j$
$-0.054 + 0.093j$	$-0.118 - 0.132j$	$-0.011 + 0.0204j$

$$\mathbf{W}_{\mathrm{A}} = \begin{bmatrix} 1 & -1 & -1 & -1 & -1 & 1 & -1 & -1 \\ -1 & 1 & 1 & 1 & 1 & -1 & 1 & 1 \\ -1 & 1 & 1 & 1 & 1 & -1 & 1 & 1 \\ -1 & 1 & 1 & 1 & 1 & -1 & 1 & 1 \\ -1 & -1 & 1 & -1 & 1 & 1 & 1 & -1 \\ 1 & 1 & -1 & 1 & -1 & -1 & -1 & 1 \\ -1 & -1 & 1 & -1 & 1 & 1 & 1 & -1 \\ -1 & -1 & 1 & -1 & 1 & 1 & 1 & -1 \end{bmatrix}, \quad \mathbf{W}_{\mathrm{B}} = \begin{bmatrix} 1 & -1 & -1 & -1 & -1 & 1 & -1 & -1 \\ 1 & -1 & -1 & -1 & -1 & 1 & -1 & -1 \\ -1 & 1 & 1 & 1 & 1 & -1 & 1 & 1 \\ 1 & -1 & -1 & -1 & -1 & 1 & -1 & -1 \\ -1 & -1 & 1 & -1 & 1 & 1 & 1 & -1 \\ -1 & -1 & 1 & -1 & 1 & 1 & 1 & -1 \\ -1 & -1 & 1 & -1 & 1 & 1 & 1 & -1 \\ 1 & 1 & -1 & 1 & -1 & -1 & -1 & 1 \end{bmatrix} \tag{46}$$

TABLE II: Array parameters considered for the example.

Attribute	Value
Array size ($M \times N$)	8×8 elements
Subarray size	2×1 elements
Polarizations	Two orthogonal
Element pattern (both polarizations)	Gaussian
Element HPBW, elevation	90°
Element HPBW, azimuth	90°
Column separation d_{y}	0.5λ
Row separation (for URA) d_{z}	0.6λ
Target beam pattern shape	Gaussian
Target HPBW, elevation	15°
Target HPBW, azimuth	65°
Electrical array tilt	6°
Electrical sub-array tilt	6°
Inter-site distance	500 m
Cell hole radius	25 m
Building height	20 m
BS height	25 m
BS power P_{BS}	46 dBm
Number of UE drops per cell	~ 7400
Number of UE antennas	2, orthogonal polariz.
UE antenna gain	0 dBi
Height outdoor UE	1.5 m
Height indoor UE	Uniform within building
Indoor UEs	80 %
Lognormal fading	6 dB
Angular spread (elevation and azimuth)	Uniform$(2^\circ, 5^\circ)$
Frequency	3.5 GHz
Pathloss model	From TR 38.901 [23]
Scenario	3GPP UMa [23]

B. Design of a Realistic Cell-Specific Beam

The above results show that, even though the conclusions of [6] hold for SPBF, it is indeed possible achieve omnidirectional transmission by using DPBF with ASI beamforming (provided that the subelement also has omnidirectional radiation pattern). However, this is rarely required in practice. Instead, one typically needs to design a cell-specific beam with certain characteristics for a specified antenna array at the base station (BS). In this section, we present an example of such practical beam design with a detailed discussion below.

Consider a typical cellular deployment with three sectors. To cover each sector, an angular range of 120° should be covered with a single beam. To avoid interference to the neighboring sectors, the beam should have a matching angular width at the level of -10 dB with respect to the beam peak. Provided that such a beam has a smooth Gaussian shape, the HPBW of such a beam should be roughly 65°.[2] The radiation pattern of a single cross-pole element typically has half-power beamwidth (HPBW) of 90° or even wider, which is too broad for sector coverage. Meanwhile, the DFT beam produced by a ULA with $N = 8$ antennas has HPBW of $\sim 10^\circ$, which is too narrow. Therefore, we need to optimize the beam pattern to find an intermediate configuration with the desired HPBW of 65°.

The array configuration and deployment of interest are summarized in Table II. Note that in contrast to the azimuth dimension, where UEs are spread widely over the entire 120°-wide sector, in the elevation dimension, UEs are located within a rather narrow angular sector. Hence, a narrow radiation pattern is required in elevation, pointing at the center of the UE distribution, as seen from the BS. In practice, this is often achieved by means of *virtualization*, i.e., partitioning the entire array into subarrays and treating those as array elements, as well as applying a tilt angle. This means that our $M \times N$ array will be reduced to an array of size $M/2 \times N$ whose elements will be subarrays of size 2×1 with pattern down-tilted by 6°. Again, according to the pattern multiplication property, the total radiation pattern of the array is given by the product of the array factor and the pattern of the subarray.

1) SPBF radiation patterns: For the case of SPBF, the beam pattern for the sector-wide public-channel transmission is optimized separately for elevation and azimuth patterns. In principle, to find the beamforming matrices for a URA with $M \times N$ dual-polarized elements one could run the optimization for the entire 2D-array. However, that is a difficult and time consuming task due to the large number of parameters. To simplify the former, we treat the total radiation pattern is a combination of the elevation pattern and the azimuth pattern. Therefore, we can optimize beamforming vectors for elevation and azimuth separately, thereby significantly reducing the computational complexity.

Assume that $\mathbf{w}_{\mathrm{y}} \in \mathbb{C}^N$ and $\mathbf{w}_{\mathrm{z}} \in \mathbb{C}^M$ are optimized beamforming vectors in azimuth and elevation dimensions, respectively. The optimized SPBF beamforming matrix of the entire two-dimensional array is then given by

$$\mathbf{W} = \mathbf{w}_{\mathrm{z}} \mathbf{w}_{\mathrm{y}}^T \in \mathbb{C}^{M \times N}. \tag{47}$$

The corresponding vector feeding the elements is found via

$$\mathbf{w}_{\mathrm{z}} = \mathbf{w}_{\mathrm{z},1} \otimes [1, 1]^T \in \mathbb{C}^M. \tag{48}$$

We consider several state-of-the-art methods to obtain weights $\mathbf{w}_{\mathrm{z},1}$ and $\mathbf{w}_{\mathrm{y}}$ suitable for cell coverage. The details of the methods and the obtained beamforming weights are presented in the appendix.

As both $\mathbf{w}_{\mathrm{z}}$ and $\mathbf{w}_{\mathrm{y}}$ are SPBF vectors the excitation matrix for the two-dimensional array $\mathbf{W}$, (47), will also be SPBF.

[2]The Gaussian shape has been selected as the target shape not because it is seen as optimal but rather due to the fact that it is widely used in practice, see, e.g., 3GPP specifications [23], [24].

Thus, only half of the elements, and hence PAs, in the array will be in use. For that reason, we feed also the orthogonal polarization B using the same excitation matrix as for the first polarization A.

Finally, we apply a scaling factor, α, to the total excitation matrix, which takes BS output power from Table II and taper loss (50) into account,

$$\alpha = \frac{\sqrt{P_{\text{BS}}/L_{\text{taper}}}}{\|[\text{vec}^T(\mathbf{W}_\text{A}), \text{vec}^T(\mathbf{W}_\text{B})]^T\|}, \tag{49}$$

This scaling factor ensures the correct output power without overloading any PA. In addition, we also need to apply the tilt according to Table II.

2) DPBF radiation patterns: The process of deriving excitation matrices for DPBF is similar to the one for SPBF patterns, but there are some important differences. One is that we now have two matrices, one per element polarization, for both elevation and azimuth beamforming. Another one is that, when creating the matrices for the entire two-dimensional array, one must avoid introducing amplitude variations.

Here we are not aiming at creating flat array factor, hence it does not suffice to only expand a single element. Instead we need to optimize the shape of the elevation DPBF beam. This is done by employing the GO method with the constraints that the excitation weights shall have constant modulus (i.e., phase-only taper) and that the elevation power pattern shall be symmetrical with respect to its peak. The optimizations are run with two objectives:

- Variance of the difference, in dB, between a target power pattern and the synthesized total power pattern within a certain angular range;
- Power utilization, which is captured by the taper loss defined as

$$L_{\text{taper}}(\mathbf{W}_\text{A}, \mathbf{W}_\text{B}) = \frac{2MN \max\{|[\text{vec}^T(\mathbf{W}_\text{A}), \text{vec}^T(\mathbf{W}_\text{B})]^T|^2\}}{\|[\text{vec}^T(\mathbf{W}_\text{A}), \text{vec}^T(\mathbf{W}_\text{B})]^T\|^2}. \tag{50}$$

The following DPBF beamforming vector is used to feed the 4 subarrays for polarization A,

$$\mathbf{w}_{\text{z,1,A}}^{\text{DP}} = \begin{bmatrix} 0.271 + 0.227j \\ 0.181 + 0.304j \\ -0.091 + 0.342j \\ -0.199 + 0.292j \end{bmatrix}. \tag{51}$$

The corresponding vector for the 8 subelements is found via

$$\mathbf{w}_{\text{z,A}}^{\text{DP}} = \mathbf{w}_{\text{z,1,A}}^{\text{DP}} \otimes [1, 1]^T \in \mathbb{C}^M. \tag{52}$$

For polarization B, the beamforming vector is defined as

$$\mathbf{w}_{\text{z,B}}^{\text{DP}} = (\mathbf{w}_{\text{z,A}}^{\text{DP}})^*. \tag{53}$$

to meet the symmetry requirement for the total power pattern.

In azimuth, a constant-modulus beamforming vector for a protoarray consisting of two dual polarized elements is found via a bisection search, similarly to what was done in [25]. Requiring that the total power pattern shall be symmetrical, the resulting vectors are

$$\mathbf{w}_{\text{y,A}}^{\text{DP}} = \begin{bmatrix} 0.458 - 0.200j \\ 0.458 + 0.200j \end{bmatrix}, \tag{54}$$

$$\mathbf{w}_{\text{y,B}}^{\text{DP}} = (\mathbf{w}_{\text{y,A}}^{\text{DP}})^*. \tag{55}$$

Next, these beamforming vectors are expanded according to Algorithm 1 to length 4, i.e., $k = 1$, and zero padded to the full length of 8. Avoiding extending the weight vector to the full length of the array and zero padding instead, is important to avoid introducing amplitude variations when the excitation matrix for the entire two-dimensional array is created (see [19] for more details).

The matrices, one per element polarization, for the entire two-dimensional array are found as

$$\mathbf{W}_\text{A}^{\text{DP}} = \mathbf{w}_{\text{z,A}}^{\text{DP}}(\mathbf{w}_{\text{y,A}}^{\text{DP}})^T - \mathbf{w}_{\text{z,B}}^{\text{DP}}(\mathbf{w}_{\text{y,B}}^{\text{DP}})^H \mathbf{J} \in \mathbb{C}^{M \times N}, \tag{56}$$

$$\mathbf{W}_\text{B}^{\text{DP}} = \mathbf{w}_{\text{z,A}}^{\text{DP}}(\mathbf{w}_{\text{y,B}}^{\text{DP}})^T + \mathbf{w}_{\text{z,B}}^{\text{DP}}(\mathbf{w}_{\text{y,A}}^{\text{DP}})^H \mathbf{J} \in \mathbb{C}^{M \times N}. \tag{57}$$

The weights are furthermore properly normalized with a scaling factor, (49), to have the correct output power without overloading any PA. In addition, a tilt is applied according to Table II.

The radiation patterns for the optimized weights of the considered methods are plotted in Fig. 7,[3] alongside the target patterns used for the beam design. Note that the elevation cuts in Fig. 7a are shown after applying the electrical tilt according to Table II.

From Fig. 7 it can be seen that the PM solution [9] provides very good matching between the beam shape and the design target. This, however, comes at the cost of poor PA utilization due to the required amplitude tapering. Hence, a certain amount of power remains unused, resulting in a taper loss. Meanwhile, the BF approach [16], being a phase tapering method, exhibits full PA utilization. Unfortunately, this comes at the cost of a certain amount of ripple present in the beam shape. The GO solution [22] does a slightly better job, providing a compromise between the two objectives: matching the beam shape to the target and the taper loss. Finally, the proposed DPBF solution with ASI beamforming, due to the additional degrees of freedom, coming from the polarization diversity, is able to match well the target beam shape, whilst remaining a phase-only approach and hence retaining full PA utilization.

3) Received signal power: To illustrate the performance gain obtained from the proposed technique, we simulate a system with a total of 27 cells in an Urban Macro (UMa) environment [23]. All BSs are equipped with the same antenna array and hence have the same beam pattern. UEs are dropped with uniform distribution in the horizontal plane, although avoiding the cell hole of 25 m around the BS. 80% of the users are located indoors and for these the height is given by a uniform distribution within $[0, \text{building height}]$. Users are served by the cell with the highest pathgain. An example of network layout is shown in Fig. 8. The figure shows the positions of 9 three-sector sites. The blue arrows in the figure

[3]See the appendix for the details of the considered state-of-the-art methods and the exact weight vectors utilized herein.

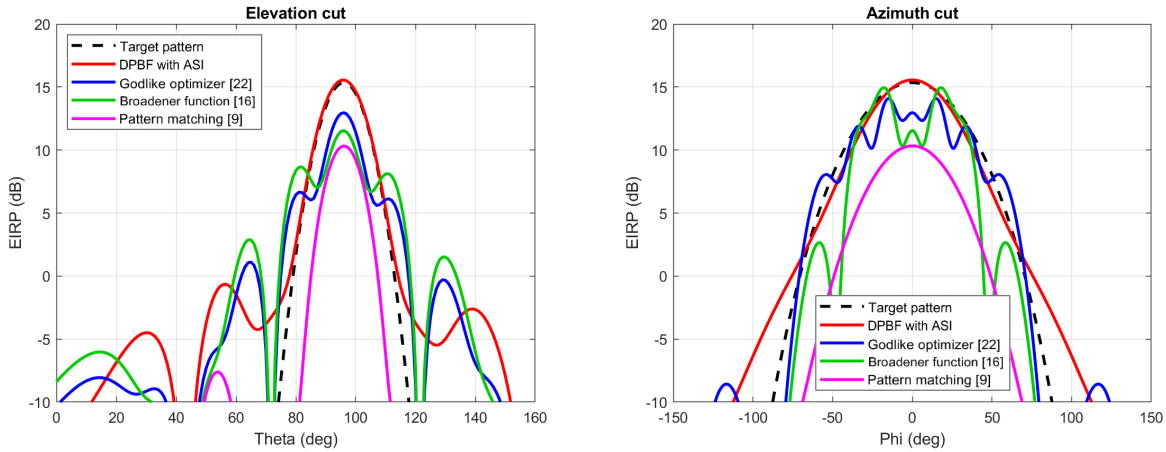

(a) Elevation cut. (b) Azimuth cut.

Fig. 7: Elevation and azimuth cuts for the optimized beam patterns.

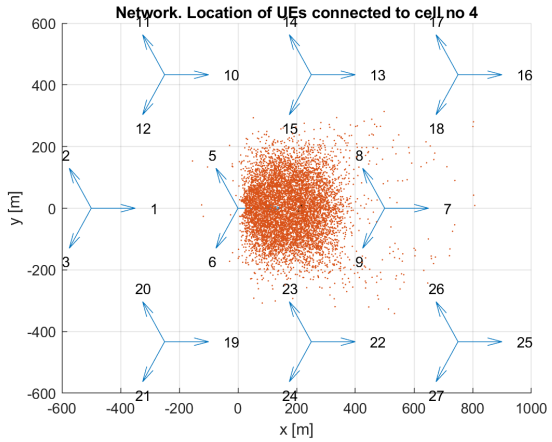

Fig. 8: Network deployment and UE locations for a DPBF serving beam.

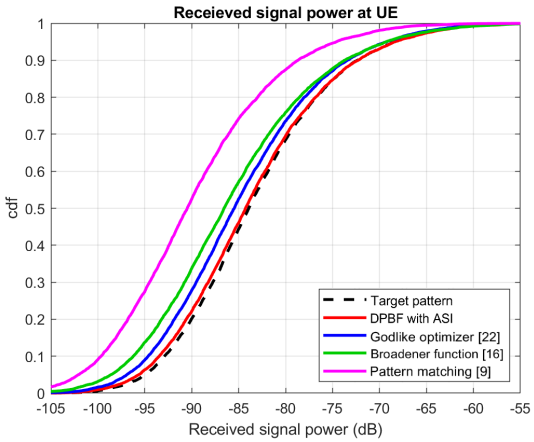

Fig. 9: Performance comparison of the proposed DPBF-based solution with ASI vs. baseline SPBF methods.

indicate the boresight directions of the antenna arrays, while the orange dots indicate the UE locations for users connected to a particular cell. As connections are based on pathgain, i.e., the combination of antenna gain and pathloss, the locations of UEs connected to a certain site depend on the shape of the serving beam. Fig. 8 shows, just as an example, the UE locations for the case of a DPBF beam.

Received signal power, i.e., the total received power of the desired signal, is used as a performance metric whose cumulative distributions for the different beamforming methods are shown in Fig. 9. The figure shows that the proposed DPBF-based ASI beamformer outperforms the SPBF solutions and approaches the upper bound, given by the performance of the ideal Gaussian beam transmitted with full power from a single hypothetical antenna. The former shows a gain of 1-1.5 dB in received signal power with respect to the best performing SPBF approach (i.e., GO beamformer). This is partly explained by the taper loss (50) of 1.1 dB for the GO solution. Furthermore, the gain comes also partly due to the better shape of the resulting power pattern of the DPBF beamformer. The other two approaches, PM and BF, perform even worse than the GO method, as seen from Fig. 9. All in all, the figure demonstrates the superiority of the proposed DPBF- and ASI-based beam design.

4) Energy efficiency: So far, we have shown the benefits of the DPBF in terms of design flexibility and improved coverage. In this subsection, we will investigate the energy efficiency of the proposed method with respect to baseline SPBF approaches. Energy efficiency can be evaluated in various ways; here, however, we have selected to compare the BS energy consumption given a certain amount of output energy. We have used the power model from [26] for which the consumed power is a linear function of the output power plus an additional baseline power consumption. That is, given the output power P_{out}, the input power is given by

$$P_{\text{in}} = P_0 + \frac{P_{\text{out}}}{\eta}, \tag{58}$$

where P_0 is the baseline power consumption and η is the power efficiency.

TABLE III: Energy efficiency metrics: taper loss, L_{taper}, input power, P_{in}, and relative energy consumption, ε_{in}.

Method	L_{taper} [dB]	P_{in} [W]	ε_{in}
DPBF with ASI	0	420	1
Broadener function [16]	0	420	1
Godlike optimizer [22]	1.1	385	1.2
Pattern matching [9]	6.6	295	3.2

Following [26, Tab. 1], the baseline power consumption P_0 is assumed to be 260 W, whereas power efficiency, denoted as η, is assumed to be 25%. As mentioned before, some of the evaluated methods suffer from taper loss (50), i.e., the output power is given by $P_{\text{out}} = P_{\text{BS}}/L_{\text{taper}}$, where $P_{\text{BS}} = 40$ W (i.e., 46 dBm; cf. Table II) is the full available power of a BS. Due to the taper loss, these methods cannot deliver full output power during the broad-beam transmission. To reach the same amount of output energy, E_{out}, the methods suffering from taper loss are required to transmit for a longer time to compensate for the lower output power. The relative increase in time is inversely proportional to L_{taper}. The consumed energy, E_{in}, over a certain transmission time interval, and the output energy are related as

$$E_{\text{in}} = \left(\frac{P_0}{P_{\text{BS}}/L_{\text{taper}}} + \frac{1}{\eta} \right) E_{\text{out}}. \tag{59}$$

Thus, the relative energy consumption, ε_{in}, defined as the energy consumption given taper loss L_{taper} vs. the case with no taper loss (i.e., $L_{\text{taper}} = 1$) for the same output energy becomes

$$\varepsilon_{\text{in}} = \frac{\eta P_0 L_{\text{taper}} + P_{\text{BS}}}{\eta P_0 + P_{\text{BS}}}. \tag{60}$$

Table III summarizes the performance of the considered methods in terms of energy efficiency. As can be seen from the table, both amplitude-tapering methods (GO and PM) exhibit significantly higher energy consumption. Hence, due to the reduced output power, they also require longer time for transmission (i.e., more retransmissions). Meanwhile, the methods involving phase-only beamforming (i.e., DPBF with ASI, as well as BF) do not incur additional energy consumption due to the absence of taper loss.

All in all, taking into account the results reported in Fig. 9 and Table III, the proposed DPBF solution with ASI beamforming exhibits the best performance when considering *both* coverage and energy efficiency.

V. Conclusion

In this paper, we have proposed the technique of array-size invariant (ASI) beamforming that allows one to expand the size of an antenna array, while preserving its total radiation pattern. The ASI technique is based on dual-polarization beamforming and successive doubling of an array, exploiting the additional degree of freedom coming from the two operating polarizations. The technique utilizes phase-only beamforming, and hence guarantees full power utilization due to constant-modulus weights. ASI beamforming is applicable to uniform linear and rectangular arrays and is characterized with simple beam synthesis. We have proposed two computationally-efficient algorithms for designing broad beams for uniform arrays of arbitrarily large size. Our numerical results and analysis demonstrate the benefits of the proposed ASI beamforming technique vs. state-of-the-art beamforming methods for designing broad beams for public-channel transmission in terms of achievable served angle range and energy consumption.

Acknowledgements

The authors would like to thank their colleagues at Ericsson Research for stimulating discussions throughout the course of this work. The anonymous reviewers are acknowledged for providing useful feedback that has significantly improved the quality of this paper.

Appendix

Herein, we discuss the details of the considered state-of-the-art methods. We also present the corresponding optimized beamforming weight vectors used for the plots in Sec. IV-B.

A. Pattern-Matching Based Beamformer

The approach of [9] allows to match the desired target pattern (ideal Gaussian pattern in our case). For a one-dimentional array, the beamforming weights are given by the roots of the following polynomial function

$$f(x) = \sum_{n=1}^{N} \mathbf{g}^T \mathbf{p}_n x^{-(N-n)} + \sum_{n=1}^{N-1} \mathbf{g}^T \mathbf{p}_{N-n}^* x^n, \tag{61}$$

where, assuming without loss of generality a horizontal array, $\mathbf{g} = [G(\phi_1), \ldots, G(\phi_{2N-1})]^T$ is the desired radiation pattern in discrete spatial directions $\phi_1, \ldots, \phi_{2N-1}$, and $\mathbf{p}_1, \ldots, \mathbf{p}_{M-1}$ are the columns of matrix $\mathbf{P} = \mathbf{V}^{-1}$, where $\mathbf{V} = [\mathbf{v}(\phi_1), \ldots, \mathbf{v}(\phi_{2N-1})]$ and

$$\mathbf{v}(\phi_k) = [e^{-j(N-1)\psi_{\text{y}}(\phi_k)}, e^{-j(N-2)\psi_{\text{y}}(\phi_k)}, \ldots, e^{-j(N+1)\psi_{\text{y}}(\phi_k)}]^T, \tag{62}$$

for all $k \in \{1, 2, \ldots, 2N-1\}$. Choosing the directions as $\phi_k = \arcsin[(2k-N)/(2N-1)]$ guarantees that $\mathbf{V}$ is invertible.

Having found roots $x_1, \ldots, x_{N-1}$ of the polynomial in (61), we obtain at most 2^{N-1} sets of beamforming weights that produce a pattern matching the target pattern $G(\phi)$. The weights are given by the coefficients of the polynomial

$$\prod_{n=1}^{N-1} (x - \alpha_n) = w_1 + w_2 x + \cdots + w_N x^{N-1}, \tag{63}$$

where $\alpha_n = x_n$ or $\alpha_n = 1/x_n^*$. Next, we loop over the obtained 2^{N-1} beamforming vectors and find the one with the lowest taper loss (50).

For the numerical example in Sec. IV-B, the resulting SPBF weight vector in azimuth is given by

$$\mathbf{w}_{\text{y}}^{\text{PM}} = \begin{bmatrix} 0.004 - 0.037j \\ -0.248 + 0.043j \\ 0.188 + 0.721j \\ 1.000 + 0.000j \\ 0.932 + 0.258j \\ 0.050 + 0.592j \\ -0.193 + 0.020j \\ 0.003 - 0.029j \end{bmatrix}. \tag{64}$$

In elevation, the obtained SPBF beamforming vector (electrical tilt not included) is

$$\mathbf{w}_{\mathrm{z},1}^{\mathrm{PM}} = \begin{bmatrix} 0.463 + 0.101j \\ 0.971 - 0.009j \\ 1.000 + 0.000j \\ 0.448 + 0.153j \end{bmatrix}. \tag{65}$$

B. Broadener-Function Based Beamformer

Another relevant method to compare against is the approach proposed in [16]. The idea is to modify a DFT weight vector with a broadener function given by

$$f_n(p,c) = \left| 4\pi c \left(\frac{2n - N + 1}{2(N-1)} \right)^p \right|, \tag{66}$$

for all $n \in \{0, \ldots, N-1\}$. Assume without loss of generality that we design a one-dimensional beam for the azimuth. Hence, after applying the broadener we get the weights

$$\mathbf{w} = [e^{jf_0(p,c)}, e^{j(f_1(p,c) - \psi_{\mathrm{y}})}, \ldots, e^{j(f_{N-1}(p,c) - (N-1)\psi_{\mathrm{y}})}]^T. \tag{67}$$

By tuning parameters (p, c) we optimize the beam shape to have a particular beamwidth. The same procedure can be applied in both dimensions of the array, and the resulting beamforming matrix for each polarization can be ontained by (47). Note that the beamforming matrix is unimodular and hence retains full power utilization.

For the numerical example in Sec. IV-B, we obtain the following SPBF beamforming vector in azimuth

$$\mathbf{w}_{\mathrm{y}}^{\mathrm{BF}} = \begin{bmatrix} -0.321 + 0.146j \\ -0.167 - 0.311j \\ 0.005 - 0.354j \\ 0.349 + 0.055j \\ 0.349 + 0.055j \\ 0.005 - 0.354j \\ -0.167 - 0.311j \\ -0.321 + 0.146j \end{bmatrix}. \tag{68}$$

When applying the above method in elevation, the obtained SPBF weight vector (subject to electrical tilt) is given by

$$\mathbf{w}_{\mathrm{z},1}^{\mathrm{BF}} = \begin{bmatrix} -0.051 + 0.497j \\ 0.499 + 0.038j \\ 0.499 + 0.038j \\ -0.051 + 0.497j \end{bmatrix}. \tag{69}$$

C. Godlike-Optimizer Based Beamformer

To optimize SPBF weights, taking into account both PA utilization and spatial ripple, we employ the robust multi-objective Godlike optimizer [22], [27]. The algorithm is based on a combination several popular optimization algorithms (i.e., Genetic Algorithm [28], Adaptive Simulated Annealing [29], Differential Evolution [30] and Particle Swarm Optimization [31]). It generates a random population of trial solutions as an initialization step. Afterwards, it partitions the population into smaller chunks, and runs a randomly chosen optimizer (out of said four) on each fraction. The output population is then be given to another optimizer, and the process is repeated until convergence. In this way, pros and cons of the algorithms compensate, thereby improving the chances of avoiding premature convergence and finding the global optimum of a non-convex optimization problem.

We run the Godlike optimizer with two said objectives

- Variance for the difference between a target pattern and the synthesized pattern within a certain angular range,
- Power variation among antennas (i.e., the taper loss).

We obtain the following SPBF weights for the numerical example in Sec. IV-B. In azimuth, the SPBF beamforming vector below is used to feed the 8 columns,

$$\mathbf{w}_{\mathrm{y}}^{\mathrm{GO}} = \begin{bmatrix} 0.189 + 0.189j \\ 0.093 - 0.165j \\ -0.244 + 0.112j \\ -0.129 + 0.232j \\ -0.129 + 0.232j \\ -0.244 + 0.112j \\ 0.093 - 0.165j \\ 0.189 + 0.189j \end{bmatrix}. \tag{70}$$

In elevation, the following beamforming vector (electrical tilt not included) is used to feed the 4 subarrays,

$$\mathbf{w}_{\mathrm{z},1}^{\mathrm{GO}} = \begin{bmatrix} 0.297 - 0.146j \\ 0.271 + 0.256j \\ 0.267 + 0.260j \\ 0.301 - 0.146j \end{bmatrix}. \tag{71}$$

REFERENCES

[1] H. Asplund *et al.*, *Advanced Antenna Systems for 5G Network Deployments: Bridging the Gap Between Theory and Practice*. Academic Press, 2020.

[2] D. J. Love and R. W. Heath, "Equal gain transmission in multiple-input multiple-output wireless systems," *IEEE Trans. Commun.*, vol. 51, no. 7, pp. 1102–1110, 2003.

[3] T. Obara, S. Suyama, J. Shen, and Y. Okumura, "Joint fixed beamforming and eigenmode precoding for super high bit rate massive MIMO systems using higher frequency bands," in *Proc. IEEE PIMRC*, 2014, pp. 607–611.

[4] T. A. Thomas, F. W. Vook, R. Ratasuk, and A. Ghosh, "Broadcast control strategies for mmWave massive MIMO leveraging orthogonal basis functions," in *Proc. IEEE Globecom*, 2015, pp. 1–6.

[5] J. Wang, H. Zhu, L. Dai, N. J. Gomes, and J. Wang, "Low-complexity beam allocation for switched-beam based multiuser massive MIMO systems," *IEEE Trans. Wireless Commun.*, vol. 15, no. 12, pp. 8236–8248, 2016.

[6] D. Qiao, H. Qian, and G. Y. Li, "Broadbeam for massive MIMO systems," *IEEE Trans. Signal Process.*, vol. 64, no. 9, pp. 2365–2374, 2016.

[7] X. Yang, W. Jiang, and B. Vucetic, "A random beamforming technique for omnidirectional coverage in multiple-antenna systems," *IEEE Trans. Veh. Technol.*, vol. 62, no. 3, pp. 1420–1425, 2012.

[8] C. Zhang, Y. Huang, Y. Jing, and L. Yang, "Energy efficient beamforming for massive MIMO public channel," *IEEE Trans. Veh. Technol.*, vol. 66, no. 11, pp. 10 595–10 600, 2017.

[9] A. Hassanien, S. A. Vorobyov, and A. Khabbazibasmenj, "Transmit radiation pattern invariance in MIMO radar with application to DOA estimation," *IEEE Signal Process. Lett.*, vol. 22, no. 10, pp. 1609–1613, 2015.

[10] V. Raghavan, J. Cezanne, S. Subramanian, A. Sampath, and O. Koymen, "Beamforming tradeoffs for initial UE discovery in millimeter-wave MIMO systems," *IEEE J. Sel. Top. Signal Process.*, vol. 10, no. 3, pp. 543–559, 2016.

[11] K. Xiong, B. Wang, C. Jiang, and K. R. Liu, "A broad beamforming approach for high-mobility communications," *IEEE Trans. Veh. Technol.*, vol. 66, no. 11, pp. 10 546–10 550, 2017.

[12] W. Fan, C. Zhang, and Y. Huang, "Flat beam design for massive MIMO systems via Riemannian optimization," *IEEE Wireless Commun. Lett.*, vol. 8, no. 1, pp. 301–304, 2018.

[13] D. Su, Y. Jiang, and X. Wang, "Semidefinite programming based omnidirectional beamforming for massive MIMO," in *Proc. IEEE WCSP*, 2017, pp. 1–6.
[14] X. Meng, X. Gao, and X.-G. Xia, "Omnidirectional precoding based transmission in massive MIMO systems," *IEEE Trans. Commun.*, vol. 64, no. 1, pp. 174–186, 2015.
[15] K. H. Sayidmarie and Q. H. Sultan, "Synthesis of wide beam array patterns using random phase weights," in *Proc. IEEE ICECCPCE*, 2013, pp. 52–57.
[16] V. Sergeev, A. Davydov, G. Morozov, O. Orhan, and W. Lee, "Enhanced precoding design with adaptive beam width for 5G new radio systems," in *Proc. IEEE VTC-Fall*, 2017, pp. 1–5.
[17] I. Tzanidis, Y. Li, G. Xu, J.-Y. Seol, and J. C. Zhang, "2D active antenna array design for FD-MIMO system and antenna virtualization techniques," *Int. J. Ant. Propag.*, vol. 2015, 2015.
[18] Z. Xiao, T. He, P. Xia, and X.-G. Xia, "Hierarchical codebook design for beamforming training in millimeter-wave communication," *IEEE Trans. Wireless Commun.*, vol. 15, pp. 3380–3392, 2016.
[19] S. O. Petersson, "Power-efficient beam pattern synthesis via dual polarization beamforming," in *Proc. EuCap 2020*, 2019.
[20] Ericsson AB, "On forming wide beams," 3GPP R1-1700772, 2017.
[21] K. Deb, "Multi-objective optimization," in *Search methodologies*. Springer, Boston, MA., 2014, pp. 403–449.
[22] R. P. Oldenhuis, "Trajectory optimization for a mission to the solar bow shock and minor planets," M.Sc. thesis, TU Dleft, 2010.
[23] 3GPP TR 38.901, "Study on channel model for frequencies from 0.5 to 100 GHz (Release 15)," 3GPP, Tech. Rep., 2018.
[24] 3GPP TR 36.873, "Study on 3D channel model for LTE (Release 12)," 3GPP, Tech. Rep., 2018.
[25] M. A. Girnyk and S. O. Petersson, "A simple cell-specific beamforming technique for multi-antenna wireless communications," in *Proc. IEEE WCNC*, 2020, pp. 1–4.
[26] P. Frenger and H. K. Wang, "Massive MIMO muting using dual-polarized and array-size invariant beamforming," in *Proc. IEEE VTC spring*, 2021, pp. 1–6.
[27] R. Oldenhuis, "Godlike—A robust single- and multi-objective optimizer," https://se.mathworks.com/matlabcentral/fileexchange/24838, 2020.
[28] D. E. Goldberg, *Genetic algorithms in search, optimization, and machine learning*. Kluwer Academic Publishers, 1989.
[29] S. Kirkpatrick, C. D. Gelatt, and M. P. Vecchi, "Optimization by simulated annealing," *Science*, vol. 220, no. 4598, pp. 671–680, 1983.
[30] D. Izzo, V. M. Becerra, D. R. Myatt, S. J. Nasuto, and J. M. Bishop, "Search space pruning and global optimisation of multiple gravity assist spacecraft trajectories," *J. Glob. Optim.*, vol. 38, no. 2, pp. 283–296, 2007.
[31] J. Kennedy and R. Eberhart, "Particle swarm optimization," in *Proc. ICNN*, vol. 4, 1995, pp. 1942–1948.

Sven O. Petersson received the M.Sc degree in Electrical Engineering from CTH (Chalmers University of Technology) in Gothenburg, Sweden, in 1979. Since 1990 he has been involved in development of base stations for various standards, and since 2001 he has been involved in research on antenna systems from 3rd till 6th generation of telecommunication systems within Ericsson Research. At present, he is working as a Master Researcher within the field of antenna systems. His current research interests are mainly related to efficient use of array antennas, including aspects such as energy efficiency, and multi-antenna transmission techniques.

Maksym A. Girnyk (S'09–M'20) received the B.Sc. and M.Sc. degrees from KPI National Technical University of Ukraine, Kyiv, Ukraine in 2005 and 2007, respectively and the M.Sc. degree from Supélec, Paris, France in 2008. Later on, he received his Lic.Eng. and Ph.D. degrees in Telecommunications from KTH Royal Institute of Technology, Stockholm, Sweden in 2012 and 2014, respectively. During this time, he held visiting appointments at the Faculty of Electrical Engineering, University of New South Wales, Sydney, Australia, the Alcatel-Lucent Chair on Flexible Radio, Supélec, Paris, France and the Department of Signal Processing and Acoustics, Aalto University, Espoo, Finland.

Since 2014, Dr. Girnyk has been working in industry, as Senior Researcher at Ericsson Research, Stockholm, Sweden, and later as Research Manager at Klarna Bank AB, Stockholm, Sweden. At present, he is working as Technical Study Driver at Ericsson Networks, Stockholm, Sweden. His research interests span several areas around 6G, including multi-antenna transmission and machine learning for radio-access networks.

Dr. Girnyk was the recipient of the IEEE VT/COM/IT Sweden Best Conference Paper Award 2015.